Available online at www.sciencedirect.com
ScienceDirect
Journal of Molecular Spectroscopy 239 (2006) 208–215
Journal of MOLECULAR SPECTROSCOPY
www.elsevier.com/locate/jms

Diode laser absorption spectrum of cold bands of C_2HD at 6500 cm^{-1}

J.L. Hardwick [a,*], Z.T. Martin [a], E.A. Schoene [b], V. Tyng [a], E.N. Wolf [a]

[a] Department of Chemistry, University of Oregon, Eugene, OR 97403-1253, USA
[b] Department of Physics, University of Oregon, Eugene, OR 97403-1253, USA

Received 13 June 2006; in revised form 14 July 2006
Available online 27 July 2006

Abstract

The absorption spectrum of acetylene-*d* has been observed at high resolution between 6470 and 6630 cm^{-1} using an external cavity diode laser. Three cold bands have been observed: the strong $2\nu_1$ band, the weaker $\nu_1 + \nu_2 + 2\nu_5$ band, and the $(\nu_1 + \nu_3 + \nu_5)^1$ band, which gains its intensity through Coriolis resonance with $2\nu_1$. Centers of unblended lines are determined with an accuracy of approximately 10 MHz.

Keywords: Acetylene-d_1; $^{12}C_2HD$; Coriolis coupling; Diode laser spectroscopy

1. Introduction

Acetylene is one of the best studied of polyatomic molecules. This is due to its importance in the chemistry of a large and diverse number of environments, to its relative ease and convenience of study, and to a variety of technological advances that have enabled observation of very high vibrational levels of this molecule.

The use by the telecommunications industry of semiconductor diode lasers between 1530 and 1565 nm (the "c-band" region) has led to a search for absolute frequency markers in this wavelength region. Among the molecules with strong spectral intensity at this wavelength, acetylene and its isotopic variants are the calibration standards of preference for many purposes. Nakagawa et al. [1] have measured the spectrum of normal acetylene ($^{12}C_2H_2$) with an absolute accuracy of 1 part in 10^9 (*ca.* 150 kHz). More recently, Edwards et al. [2] measured lines of the same band with an accuracy of 3–10 kHz using saturation spectroscopy. These studies make the spectrum of normal acetylene a useful secondary standard for spectroscopy in the 1.5 μm region.

Although the spectrum of $^{12}C_2HD$ in this region is less well studied than the main isotopomer, a vast body of literature nonetheless exists. Herzberg et al. [3] reported the infrared spectrum of this species in 1934, as did McKellar and Bradley [4]. Latrasse et al. [5] have provided Fourier transform infrared (FTIR) measurements of the $2\nu_1$ band centered at 1522 nm with an accuracy of 0.004 nm (1 part in 4×10^5), while Lievin et al. [6] have reported rotational constants and band origins for some 40 bands of $^{12}C_2HD$, including three bands in the wavenumber region addressed by this paper. Fusina et al. [7] have recently reported precise FTIR spectra of this species in the region between 1800 and 4700 cm^{-1}, and Herman et al. [8] have performed a global vibrational fit of known bands up to 24 128 cm^{-1}.

There is a small (*ca.* 0.01 D) permanent dipole moment associated with C_2HD, giving rise to a microwave spectrum. This microwave spectrum has been studied by Muenter and Laurie [9] and by Wlodarczak et al. [10], and four rotational transitions of the vibrational ground state are known with high accuracy.

The advent of commercially available tunable lasers in the 1.5 μm region of the spectrum now enables convenient inspection of this spectrum at an instrumental resolution significantly higher than that available from even the best available Fourier transform spectrometers. This improved resolution can, when properly used, provide enhanced pre-

* Corresponding author. Fax: +1 541 346 4643.
E-mail address: hardwick@uoregon.edu (J.L. Hardwick).

0022-2852/$ - see front matter © 2006 Elsevier Inc. All rights reserved.
doi:10.1016/j.jms.2006.07.008

cision and accuracy as well. We report here the high-resolution measurement of three bands of $^{12}C_2HD$ using an external cavity diode laser. The measurements cover the region from 6474 to 6632 cm^{-1} (1508–1545 nm) and the measured line centers have an estimated accuracy of 0.0003 cm^{-1}.

2. Experimental method

C_2HD was prepared by reacting ethanol-d_1, C_2H_5OD, with sodium acetylide, NaC_2H. Sodium acetylide (Sigma–Aldrich) was provided as a slurry in mineral oil and xylene. This slurry was transferred to a flask and placed under vacuum, and the high vapor pressure fraction was allowed to evaporate until the pressure remained below 1 torr. Owing to the sometimes violent reaction of NaC_2H with moisture, only amounts of ~1 g or less were used at a time. The sodium acetylide slurry was then cooled to 77 K, and ethanol-d_1 was distilled under vacuum to condense in the same flask as the sodium acetylide. The resulting mixture was slowly warmed up until reaction occurred, liberating C_2HD gas. The resulting gas was transferred into the sample cell and used without further purification, where it was found to last without deterioration for several weeks. The main contaminant was found to be ordinary acetylene.

The optical arrangement is illustrated in Fig. 1. A commercial external cavity diode laser (New Focus 6428) was coupled out through an optical fiber using an FC/APC connector to minimize optical feedback. Light from the optical fiber was collimated, and part of the collimated light was picked off by the mirror (M1) and directed through an internally coupled Fabry–Perot interferometer (FP) [11] with a free spectral range of 0.009725 cm^{-1}. Part of the remaining light was picked off using a second mirror (M2). One of the beams was passed through a 1-m reference cell filled with $^{12}C_2H_2$ at a pressure of 1–4 torr (C1), while the other was passed through a 1-m sample cell filled with $^{12}C_2HD$ at a pressure of 1–4 torr (C2). In some experiments the 1-m sample cell was replaced with a multipass white cell of 1.5-m base path set to four traversals, and the pressure was increased to as much as 30 torr to increase the intensity of high-J lines. Light was detected in each path using an InGaAs detector (ThorLabs PDA400), amplified using a home-built variable-gain preamplifier with variable offset, and recorded using an A/D converter (National Instruments PCI-6221).

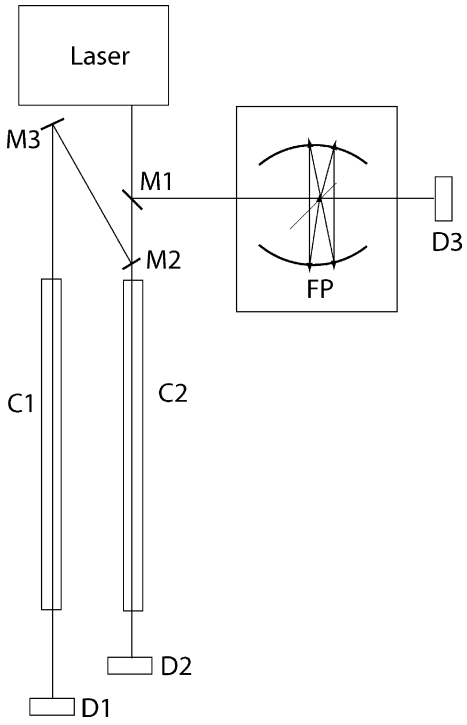

Fig. 1. A block diagram of the experiment. Light from the laser was directed through the sample cell C1 (C_2HD), the calibration cell C2 (C_2H_2), and the interferometer FP by means of the pick-off mirrors M1, M2, and M3. InGaAs detectors D1, D2, and D3 detected the incident light and transmitted the resulting signal to an analog-to-digital converter for computer processing.

The laser scanned at a rate of 1 nm/s. Scanning at this rate, the laser was found to scan reliably from 6450 to 6650 cm^{-1} without mode hops (and for wider ranges, though with less reliability). Data collection was set at 50,000 samples/s, providing a collection resolution of 8×10^{-5} cm^{-1} per data point. The Doppler width of an isolated absorption line of acetylene is 0.016 cm^{-1} at room temperature, so the profile of a single line was sampled with about 200 data points. There were about 100 points in the free spectral range of the interferometer used for calibration. Laser power was set between 0.5 and 1.0 mW.

Data collection was performed with Igor Pro (WaveMetrics, Inc.), using Igor NIDAQ Tools MX to control the interface card. Data were digitized with 16-bit resolution so that the S/N ratio was not limited by digitizing error. The noise level, which amounts to about 0.1% of the full scale signal in the sample channel, is believed to be due to a combination of laser jitter and detector noise. The laser was also controlled with Igor Pro using a GPIB interface.

The quality of the spectrum is compromised by presence of accidental etalons produced by the cell windows and other optical elements. These were minimized by using wedged windows on the absorption cells; by using pick-off mirrors (M1 and M2 in Fig. 1) instead of beam splitters; and by deliberately abrading the most troublesome optical surfaces.

Calibration of the spectrum was accomplished using the interferometer fringes to provide relative calibration frequency markers and absorption lines from normal acetylene to provide absolute frequency markers. First, a wavenumber scale was established by fitting the accurately known wavenumbers of acetylene [1,2] as a function of interferometer fringe number: the acetylene lines were fitted to a Gaussian line profile, and the line center was interpolated to find its position in 'fringe space' using a two-parameter fit, the two parameters being the free spectral range of the interferometer and the wavenumber at the first

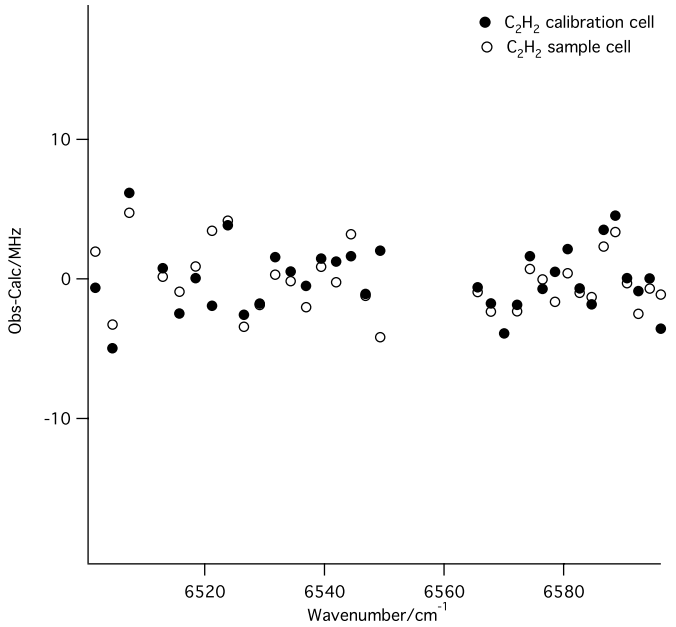

Fig. 2. Residual error of the calibration. The calibrated line centers of normal acetylene lines for a single run are subtracted from the published values of references [1,2]. Closed circles denote lines measured in the reference cell, and open circles indicate contaminant lines measured in the sample cell.

recorded fringe. The residual errors of the resulting fit are illustrated in Fig. 2, indicating a random error of about 10^{-4} cm^{-1}. The fit was insensitive to the assumed line shape of the calibration lines: the difference between line centers found using a Gaussian profile and those found using a Voigt profile was determined typically to be less than 10^{-5} cm^{-1}. The wavenumber scale was then transferred to the C_2HD spectrum, which had been recorded simultaneously with the C_2H_2 spectrum. A contaminant of normal

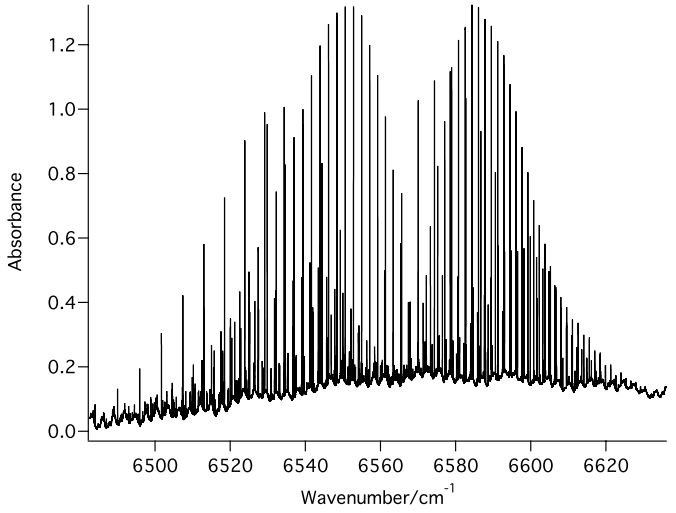

Fig. 3. An overview of the spectrum. The closely spaced band at higher wavenumber is C_2HD, while the band at lower wavenumber showing 3:1 intensity alternation is normal acetylene, C_2H_2. The oscillations in the baseline are caused by accidental etalons in the optical path (see text).

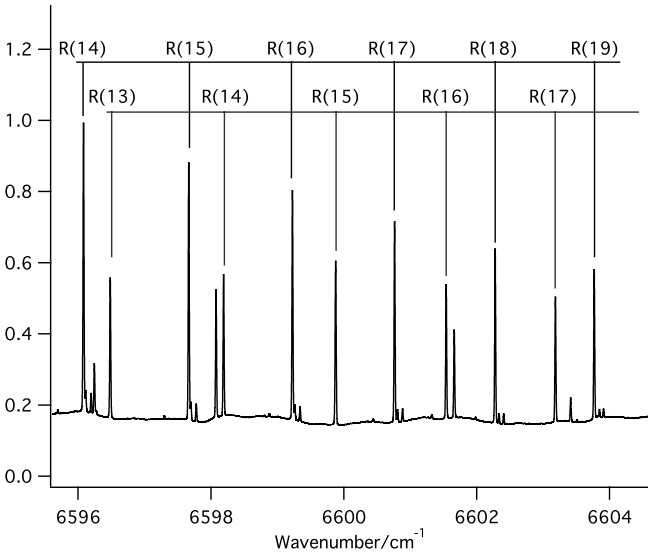

Fig. 4. A detail of the spectrum of C_2HD. The upper assignments are for the main $2\nu_1$ band, while the lower assignments are for the $\nu_1 + \nu_3 + \nu_5$ band. Weak unmarked features are largely due to hot bands of C_2HD [6].

C_2H_2 in our sample was estimated to range between 5 and 10%, based on the absolute intensity of the $\nu_1 + \nu_3$ band of C_2H_2 [12] and the $2\nu_1$ band of C_2HD [6]. This contaminant of C_2H_2 in the sample cell afforded an additional check on the calibration procedure. This check also showed residuals of about 10^{-4} cm^{-1} in magnitude; these residual errors are also illustrated in Fig. 2. The entire procedure for calibrating the spectra was largely automated using Igor Pro.

A portion of the recorded spectrum is presented in Fig. 3, and a detail illustrating line assignments is presented in Fig. 4. Isolated lines could be measured with a reproducibility of slightly better than 10^{-4} cm^{-1}.

3. Results and analysis

There are three readily identified cold bands in the region studied, all consisting of P and R branches with no Q branch. The strongest of these is the $2\nu_1$ band at 6569.42 cm^{-1}. A second, much weaker, band occurs at 6483.82 cm^{-1}; this band is assigned as $\nu_1 + \nu_2 + 2\nu_5^0$. Both of these bands have been reported by Lievin et al. [6]. The third band, whose origin is 6570.58 cm^{-1}, has not previously been reported; for reasons we discuss later we assign it as the $\nu_1 + \nu_3 + \nu_5^1$ band, which takes intensity from the $2\nu_1$ band via Coriolis resonance.

3.1. Rotational assignments and ground-state constants

Rotational assignments are presented in Table 1. The assignments for the main band were performed by inspection and were found to agree completely with those of Latrasse et al. [5]. Assignments of the weaker bands were made using the ground-state combination differences obtained from the stronger band; the combination differences from the three bands were found to agree within

Table 1
Observed lines and rotational assignments for the 1.55 μm cold bands of C_2HD

$(2,0,0,0,0)$			$(1,0,1,0,1)^1$			$(1,1,0,0,2)^0$		
J	$P(J)$	$R(J)$	J	$P(J)$	$R(J)$	J	$P(J)$	$R(J)$
0		6571.3717(−2)						
1	6567.4324(−2)	6573.3009(−4)	1			1		6487.7490(11)
2	6565.4225(−2)	6575.2043(1)	2		6576.4236(−8)	2		6489.6960(3)
3	6563.3859(−3)	6577.0807(−2)	3		6578.3405(−4)	3	6477.8334(6)	6491.6298(−18)
4	6561.3232(−1)	6578.9316(−1)	4	6562.5430(−4)	6580.2398(−2)	4	6475.8152(5)	6493.5557(2)
5	6559.2342(−1)	6580.7569(0)	5	6560.4940(−3)	6582.1210(−2)	5	6473.7848(−2)	6495.4669(−2)
6	6557.1196(0)	6582.5571(2)	6	6558.4276(−3)	6583.9840(−1)	6		6497.3663(−2)
7	6554.9798(1)	6584.3322(1)	7	6556.3442(2)	6585.8284(0)	7	6469.6896(−4)	6499.2533(−1)
8	6552.8150(0)	6586.0828(1)	8	6554.2420(−2)	6587.6537(1)	8	6467.6246(0)	6501.1270(−6)
9	6550.6258(0)	6587.8092(2)	9	6552.1221(1)	6589.4596(2)	9	6465.5471(0)	6502.9894(5)
10	6548.4125(0)	6589.5112(0)	10	6549.9833(−1)	6591.2466(9)	10	6463.4570(−4)	
11	6546.1754(0)	6591.1897(1)	11	6547.8261(2)	6593.0124(3)	11	6461.3553(−1)	6506.6717(−2)
12	6543.9150(1)	6592.8443(2)	12	6545.6497(4)	6594.7587(2)	12	6459.2413(6)	6508.4920(−10)
13	6541.6314(4)	6594.4753(2)	13	6543.4538(2)	6596.4850(4)	13	6457.1132(−1)	6510.2985(−16)
14	6539.3242(1)	6596.0827(2)	14	6541.2388(4)	6598.1907(3)	14	6454.9731(2)	6512.0934(4)
15	6536.9944(1)	6597.6666(2)	15	6539.0042(4)	6599.8769(13)	15	6452.8195(2)	6513.8719(6)
16	6534.6419(2)	6599.2271(2)	16	6536.7496(0)	6601.5405(2)	16	6450.6523(1)	6515.6340(−6)
17	6532.2666(1)	6600.7641(0)	17	6534.4761(4)	6603.1843(0)	17	6448.4710(−3)	6517.3827(1)
18	6529.8688(0)*	6602.2778(−1)	18	6532.1822(1)	6604.8074(−1)	18	6446.2771(7)	6519.1151(1)
19	6527.4486(0)	6603.7682(−1)	19	6529.8688(−1)*	6606.4098(−1)	19	6444.0677(5)	6520.8305(−8)
20	6525.0062(0)	6605.2355(1)	20	6527.5359(1)	6607.9913(−2)	20	6441.8439(7)	6522.0163()
21	6522.5413(−1)	6606.6791(−1)	21	6525.1829(−1)	6609.5517(−4)	21	6439.6042(−1)	6524.2133(−7)
22	6520.0543(−1)	6608.0996(−1)	22	6522.8102(−2)	6611.0914(−4)	22		6525.8787(−10)
23	6517.5452(−1)	6609.4967(−1)	23	6520.4179(−2)	6612.6102(−3)	23	6435.0803(2)	
24	6515.0138(−2)	6610.8704(−2)	24	6518.0055(−6)	6614.1079(−3)	24	6432.7937(−3)	
25	6512.4606(−1)	6612.2209(−1)	25	6515.5741(−3)	6615.5847(−2)	25	6430.4923(8)	
26	6509.8852(−2)	6613.5479(0)	26	6513.1227(−3)	6617.0404(−2)	26	6428.1723(1)	
27	6507.2880(−1)	6614.8515(0)	27	6510.6517(−3)	6618.4750(−3)	27	6425.8355(0)	
28	6504.6688(0)	6616.1341(25)*	28	6508.1613(−1)	6619.8887(−2)	28	6423.4812(−1)	
29	6502.0277(2)	6617.3888(5)	29	6505.6510(−3)	6621.2813(−2)	29	6421.1086(−4)	
30	6499.3678(34)*	6618.6209(−5)	30	6503.1229(12)	6622.6529(−1)			
31	6496.6799(5)	6619.8310(−1)	31	6500.5715(−11)	6624.0037(2)			
32	6493.9719(−7)	6621.0174(2)	32	6498.0041(−1)	6625.3329(−1)			
33	6491.2440(0)	6622.1800(2)	33	6495.4164(0)	6626.6416(1)			
34	6488.4937(1)	6623.3191(3)	34	6492.8094(0)	6627.9291(2)			
35	6485.7217(2)	6624.4344(2)	35	6490.1831(−1)	6629.1960(7)			
36	6482.9279(2)	6625.5260(1)	36	6487.5379(1)	6630.4415(8)			
37	6480.1112(−9)	6626.5944(4)	37	6484.8743(10)	6631.6656(4)			
38	6477.2750(1)	6627.6378(−6)	38	6482.1921(23)	6632.8701(15)			
39	6474.4162(1)	6628.6592(0)	39	6479.4876(3)	6634.0528(18)			
40		6629.6563(1)	40	6476.7662(3)	6635.2080(−45)			
41		6630.6298(4)	41		6636.3531(1)			
42	6465.7105(2)	6631.5787(−2)	42	6471.2620(−46)	6637.4725(0)			
43	6462.7651(−2)	6632.5024(−21)*	43	6468.4895(7)	6638.5707(−3)			
44			44	6465.6922(−2)	6639.6491(−3)			
45	6456.8107(−1)		45		6640.7049(−3)			
			46	6460.0449(13)				
			47	6457.1901(−13)				

All values are in units of cm^{-1}. Observed − calculated line positions are indicated in parentheses in units of the last significant figure. Overlapped lines are marked with an asterisk and were not included in the fit. Lines not listed in the table were either too weak to identify (e.g., the low-J lines of the $(1,0,1,0,1)^1$ band) or obscured by stronger lines (e.g., the $R(10)$ and $P(6)$ lines of the $(1,1,0,0,2)^0$ band).

$1.5 \times 10^{-4}\,cm^{-1}$ for unblended lines, confirming that the weaker bands also originate from the ground vibrational state of C_2HD.

Ground-state rotational constants were obtained from a least-squares fit of the ground-state combination differences of the three bands. The combination differences were weighted as the inverse of their variance, the variance being determined both from the reproducibility among the three bands and the reproducibility across several measurements of the same lines. The ground-state microwave transitions summarized by Wlodarczak et al. [10] were also included in this fit.

The rotational constants B'', D'', and H'' for the ground state are presented in Table 2; these were all found to agree

Table 2
Ground-state rotational constants for C_2HD

Constant	Present work	Reference [7]
B	0.99152629(130)	0.991527586(80)
$D/10^{-6}$	1.13568 (104)	1.13531(27)
$H/10^{-12}$	1.24(34)	1.17(11)

All values are given in units of cm^{-1}. Statistical estimates of uncertainties (one standard deviation) are presented in parentheses in units of the last significant figure of the corresponding constant.

within our estimated uncertainty with those presented by Fusina et al. [7]. Inasmuch as the constants presented by Fusina are drawn from many more bands and thus have a smaller standard error, those constants were used for the subsequent analysis of the upper state.

3.2. Upper-state rotational analysis

The upper states were rotationally analyzed by fitting the upper-state term values. These term values were constructed by computing the ground-state term values from the constants of Fusina et al. from Table 2, then adding these to the line positions of Table 1.

Analysis of the $(1,1,0,0,2)^0$ state was straightforward and presented no difficulties. The rotational constants for this state are presented in Table 3.

Rotational analyses of the upper states of the $(2,0,0,0,0)^0$ and $(1,0,1,0,1)^1$ states must be performed simultaneously. As shown by Lievin et al. [6], analysis of the $(2,0,0,0,0)^0$ state without explicitly considering the perturbation by the neighboring state leads to a slowly converging series in $J(J+1)$ involving effective centrifugal distortion constants, including a negative value of D'. Such a series is characteristic of a perturbed state. The weaker band appears to concentrate its intensity in somewhat higher J lines than the stronger band: the strong band has its peak intensity at $P(9)$ and $R(8)$, while the weak band peaks at $P(14)$ and $R(10)$. Moreover, the relative intensities of the two bands are strongly J-dependent: the $\nu_1+\nu_3+\nu_5$ band has only about 15% of the intensity of the $2\nu_1$ band at $J=8$, while at $J=30$ the intensities are approximately equal. These observations indicate the two levels are in resonance, with the weaker transition drawing intensity from the more intense band.

The parameters that are spectroscopically determinable are not obvious, but they may be deduced by examining the eigenvalues of the coupled Hamiltonian. The Hamiltonian matrix for a Σ and Π state in Coriolis resonance is [13]

$$H=\begin{pmatrix} H_{1,1} & \xi\sqrt{J(J+1)} \\ \xi\sqrt{J(J+1)} & H_{2,2}\end{pmatrix}, \tag{1}$$

where the diagonal matrix elements of Eq. (1) are given by

$$\begin{aligned} H_{1,1} &= \nu_0^{\Sigma}+B_{\Sigma}J(J+1)-D_{\Sigma}[J(J+1)]^2 \\ &\quad +H_{\Sigma}[J(J+1)]^3+L_{\Sigma}[J(J+1)]^4+\cdots \\ H_{2,2} &= \nu_0^{\Pi}+B_{\Pi}[J(J+1)-1]-D_{\Pi}[J(J+1)-1]^2 \\ &\quad +H_{\Pi}[J(J+1)-1]^3+L_{\Pi}[J(J+1)-1]^4+\cdots \end{aligned} \tag{2}$$

and ξ is an anharmonic Coriolis coupling coefficient. Since the observed transitions are all e–e transitions, we are unable to determine the ℓ-type doubling coefficient q, so B_{Π} also contains the effect of q. The diagonal matrix element for the Π state through terms in L may be rewritten in the same form as that of the Σ state by making the following definitions:

$$\begin{aligned} \nu_{\Pi}^{\text{eff}} &= \nu_0^{\Pi}-B_{\Pi}-D_{\Pi}-H_{\Pi}+L_{\Pi}, \\ B_{\Pi}^{\text{eff}} &= B_{\Pi}+2D_{\Pi}+3H_{\Pi}-4L_{\Pi}, \\ D_{\Pi}^{\text{eff}} &= D_{\Pi}+3H_{\Pi}-6L_{\Pi}, \\ H_{\Pi}^{\text{eff}} &= H_{\Pi}-4L_{\Pi}, \\ L_{\Pi}^{\text{eff}} &= L_{\Pi} \end{aligned} \tag{3}$$

so that

$$\begin{aligned} H_{2,2} &= \nu_{\Pi}^{\text{eff}}+B_{\Pi}^{\text{eff}}J(J+1)-D_{\Pi}^{\text{eff}}[J(J+1)]^2 \\ &\quad +H_{\Pi}^{\text{eff}}[J(J+1)]^3+\cdots. \end{aligned} \tag{4}$$

The eigenvalues of the Hamiltonian matrix for the coupled states are

$$E_{\pm}=\frac{1}{2}\left(H_{1,1}+H_{2,2}\pm\sqrt{(H_{1,1}-H_{2,2})^2+4\xi^2J(J+1)}\right). \tag{5}$$

There are two combinations of these eigenvalues that yield simple power series expansions in $J(J+1)$:

$$\begin{aligned} \tfrac{1}{2}(E_++E_-) &= \tfrac{1}{2}(H_{1,1}+H_{2,2}) \\ &= \overline{\nu}+\overline{B}J(J+1)-\overline{D}[J(J+1)]^2 \\ &\quad +\overline{H}[J(J+1)]^3+\overline{L}[J(J+1)]^4+\cdots \end{aligned} \tag{6}$$

and

$$\begin{aligned} (E_+-E_-)^2 &= (H_{1,1}-H_{2,2})^2+4\xi^2J(J+1) \\ &= \Delta\nu^2+(2\Delta B\Delta\nu+4\xi^2)J(J+1) \\ &\quad -(2\Delta D\Delta\nu-\Delta B^2)[J(J+1)]^2 \\ &\quad +(2\Delta H\Delta\nu-2\Delta B\Delta D)[J(J+1)]^3 \\ &\quad +(\Delta D^2+2\Delta B\Delta H+2\Delta L\Delta\nu)[J(J+1)]^4 \\ &\quad +(2\Delta B\Delta L-2\Delta D\Delta H)[J(J+1)]^5 \\ &\quad +(\Delta H^2-2\Delta D\Delta L)[J(J+1)]^6+\cdots \end{aligned} \tag{7}$$

Table 3
Rotational constants for the $(1,1,0,0,2)^0$ state of C_2HD

Constant	Present work	Reference [7]
ν_0	6483.81697(20)	6483.82161(50)
B	0.9856802(23)	0.9856749(41)
$D/10^{-6}$	2.0378(64)	1.9806(62)
$H/10^{-12}$	62.98(465)	

All values are given in units of cm^{-1}. Statistical estimates of uncertainties (one standard deviation) are presented in parentheses in units of the last significant figure of the corresponding constant.

with

$$\begin{aligned}
\overline{\nu} &= \frac{1}{2}(\nu_0^{\Sigma} + \nu_{\Pi}^{\mathrm{eff}}) \quad \Delta\nu = \nu_0^{\Sigma} - \nu_{\Pi}^{\mathrm{eff}},\\
\overline{B} &= \frac{1}{2}(B_{\Sigma} + B_{\Pi}^{\mathrm{eff}}) \quad \Delta B = B_{\Sigma} - B_{\Pi}^{\mathrm{eff}},\\
\overline{D} &= \frac{1}{2}(D_{\Sigma} + D_{\Pi}^{\mathrm{eff}}) \quad \Delta D = D_{\Sigma} - D_{\Pi}^{\mathrm{eff}},\\
\overline{H} &= \frac{1}{2}(H_{\Sigma} + H_{\Pi}^{\mathrm{eff}}) \quad \Delta H = H_{\Sigma} - H_{\Pi}^{\mathrm{eff}},\\
\overline{L} &= \frac{1}{2}(L_{\Sigma} + L_{\Pi}^{\mathrm{eff}}) \quad \Delta L = L_{\Sigma} - L_{\Pi}^{\mathrm{eff}}.
\end{aligned} \tag{8}$$

It should be clear from the foregoing that not all the parameters will be determinable from these data. In particular, ΔB and ξ are coupled by the data set, as are ΔB and ΔD; ΔD and ΔH; and so on. Parameters thus coupled cannot generally be determined simultaneously without additional information or simplifying assumptions.

In the present case $\Delta\nu$ is found to be about 1.15 cm^{-1}. Based on the vibrational ground states of normal and deuterated acetylene, B, D, and H are approximately 1, 10^{-6}, and 10^{-12} cm^{-1}, respectively. ΔB is expected to be about 10^{-2} cm^{-1}, while ΔD and ΔH are expected to be of the same order as the constants themselves. Based strictly on the intensities of the two bands as a function of J, the anharmonic Coriolis coupling coefficient is expected to lie between 0.01 and 0.1 cm^{-1}. Accordingly, the coefficient in Eq. (7) that multiplies $J(J+1)$ will consist of two terms comparable in magnitude, and the coefficient multiplying $[J(J+1)]^2$ is dominated by ΔB^2.

We have adopted the expedient of setting $\Delta L = 0$, and this assumption appears to be justified by the small magnitude of ΔD and ΔH in the final fit. We have further assumed that any centrifugal correction to the Coriolis coupling constant ξ can be neglected. Based on these assumptions, rotational constants for the coupled states were determined using a nonlinear least-squares fit. These constants are presented in Table 4.

Table 4
Rotational constants for the $(2,0,0,0,0)$ (Σ) and $(1,0,1,0,1)^{1e}(\Pi^e)$ states of C_2HD

Constant	Present work	Reference [7]
ν_{Σ}	6569.41566(20)	6569.4102(11)
ν_{Π}	6571.55529(25)	
B_{Σ}	0.9799326(92)	0.978480(14)
B_{Π}^{e}	0.9815489(93)	
$D_{\Sigma}/10^{-6}$	1.1579(63)	−0.493(43)
$D_{\Pi}^{e}/10^{-6}$	1.1250(68)	
$H_{\Sigma}/10^{-12}$	13.16(258)	−1050(46)
$H_{\Pi}^{e}/10^{-12}$	9.56(300)	
$L/10^{-15}$	−1.63(63)	261(15)
ξ	0.04616(1)	

All values are given in units of cm^{-1}. Statistical estimates of uncertainties (one standard deviation) are presented in parentheses in units of the last significant figure of the corresponding constant.

3.3. Vibrational assignment of the perturbing state

Our assignment of the vibrational quantum numbers of the perturbing state rests on three independent features: the intensity distribution of rotational lines in the perturbing band, the deperturbed rotational constants, and the band origin of the perturbing state.

The intensity distribution of the perturbing band is inconsistent with a homogeneous perturbation (i.e., one whose coupling matrix element is independent of rotational quantum number). If the coupling were independent of rotational quantum number, the intensity would be dictated entirely by the energy difference of interacting states, and we would observe the maximum 'borrowing' of intensity where the lines of the bright state and the dark state are closest together. If, on the other hand, the perturbation increases with J, the intensity borrowed by the dark state will increase with the magnitude of the coupling element, and the intensity will increase as the levels are pushed apart. The latter case is observed, strongly indicating that we are observing a Coriolis perturbation, and that the perturbing state has Π_u vibrational symmetry.

The deperturbed rotational constants can be predicted from the values of B_0, α_i, and γ_{ij} reported previously [7,8,14]. The observed and predicted B values for the $(1,0,1,0,1)$ state are 0.98183 and 0.98155 cm^{-1}, respectively. The difference of 0.0003 cm^{-1} is comparable to the residual obtained from other overtone and combination bands using these constants. The vibrational term value may be calculated using the constants of Herman et al., either as a Dunham expansion or including the off-diagonal term due to the $K_{1/255}$ resonance. The calculated range of 6572.51–6571.70 cm^{-1} is again acceptably close to our observed value of 6571.55529 cm^{-1}. Indeed, such a good agreement may be accidental, since the work to date has been unable to determine values for some of the constants (e.g., y_{133}) necessary to predict this term value accurately. Still, there is no obvious alternative candidate for the perturbing state.

4. Discussion

Absorption spectroscopy is broadly complementary to dispersed fluorescence and stimulated emission pumping spectroscopy, inasmuch as it provides the same kind of information on a different set of excited states. Numerous examples of Coriolis coupling have been reported for normal acetylene, both in absorption and in other techniques, so the present case comes as no surprise. Indeed, rotational perturbations have been identified in higher vibrational levels of C_2HD, although the perturbing state has so far resisted analysis [15].

The accuracy of the reported lines is typically 10 MHz. Where lines are overlapped the uncertainty is somewhat greater, and these are indicated in Table 1. There could be some systematic shift of lines in our high pressure spectra. For normal acetylene Swan and Gilbert [16] have

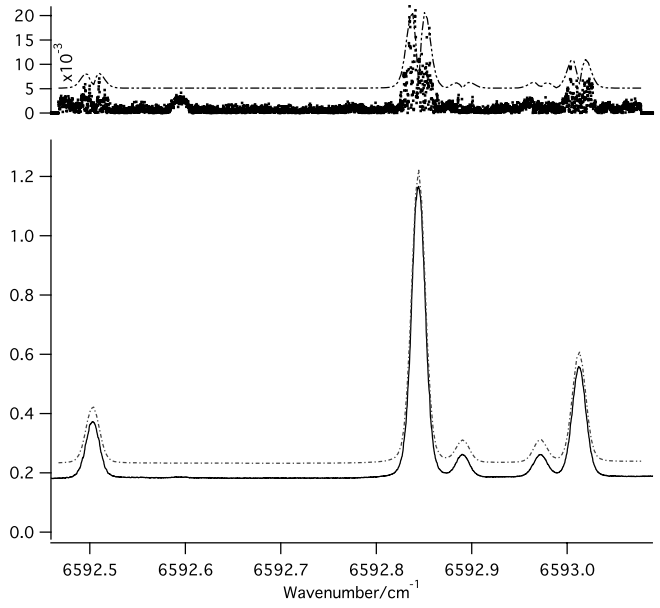

Fig. 5. The effect of laser wavelength instability on the observed spectrum of C_2HD. The lower traces are the experimental spectrum (solid trace) converted to absorbance and a fit of that spectrum (dotted line) to Voigt profiles. The upper part of the figure shows the absolute value of the residual error of the fit (scatter plot) and the absolute value of the first derivative of the fit (dotted line) multiplied by the estimated laser jitter of 10^{-4} cm^{-1}. Model traces have been offset from zero for clarity. As shown by the agreement between the upper two traces, virtually all of the discrepancy between the fitted lines and the observed spectrum is due to wavelength jitter.

reported pressure shifts of up to −0.73 MHz/torr at $J'' = 27$. Moreover, the shifts reported by Swan and Gilbert are most important for high-J lines, which are best determined in C_2HD from our high pressure spectra. Accordingly, we assign a somewhat greater uncertainty of 20 MHz to transitions with $J > 30$. The pressure shift for the P and R branches of the same J should be comparable, and so we expect this source of error will not affect the ground-state combination differences noticeably.

The source of wavenumber error can be traced in large part to wavelength jitter of the laser. We have fitted the absorbance of several lines in a small part of the spectrum to Voigt profiles; this plot is shown in Fig. 5. An examination of the residual error of the fit reveals that the noise is greatest where the slope of the absorption is at a maximum. If the dominant source of noise is the wavelength instability of the laser, then by the usual method of error propagation,

$$|\sigma_A| = |\sigma_\nu| \left| \frac{\partial A}{\partial \nu} \right|. \tag{9}$$

In Eq. (9), σ_A is the residual error in absorbance, σ_ν is the noise of the laser frequency during the time in which a data point is collected, and $|\frac{\partial A}{\partial \nu}|$ represents the derivative of absorbance with respect to frequency. Evaluating this derivative from our modeled line shape and multiplying by an estimated wavenumber jitter of 10^{-4} cm^{-1} leads to a model for the absolute value of the residual error in absorbance, which is shown as a dotted line at the top of Fig. 5.

The residuals obtained using the constants of Table 4 are illustrated in Fig. 6. Although the fit is adequate, it nonetheless reveals slight systematic deviations from our model. These deviations are especially evident above $J = 30$, where a second, smaller, perturbation seems to have its onset. Unfortunately, the lines at high J are weak, and so an improvement of the model is not warranted at this point. Moreover, since the observed transitions are all e–e transitions [17], information on the f-parity levels of the $(1,0,1,0,1)^1$ state are completely missing. This information will only be provided by hot band spectra from a different region.

C_2HD is of some considerable interest in its own right because of its isotope-dependent photochemistry. Arusi-Parpar et al. [18] have noted that there is a substantial rota-

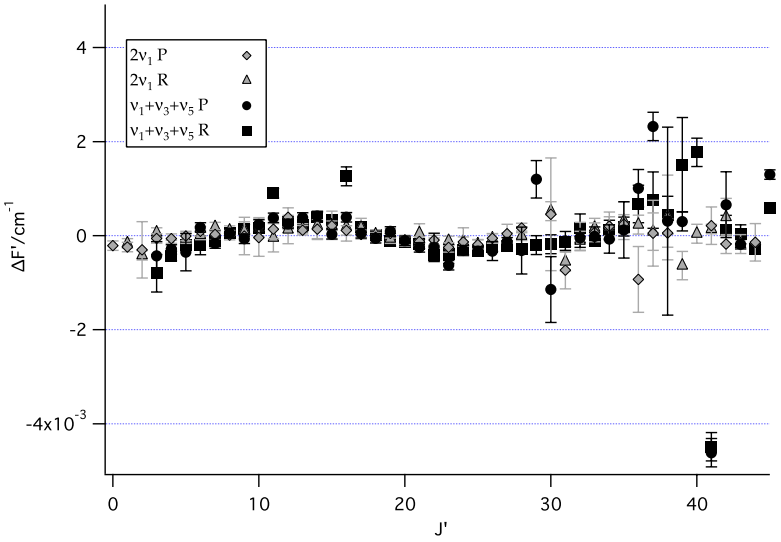

Fig. 6. Residual error of the fit of the two Corolis coupled bands of C_2HD. The lower state is taken as fixed, and the observed − calculated upper-state term values are plotted as a function of J'.

tional dependence to the H/D branching ratio in the photolysis of C_2HD, and that this rotational dependence is likely caused by local perturbations that mix the pure C–H stretch with other vibrational degrees of freedom. While the present results do not speak directly to their experiment, they do demonstrate a rotation-dependent mixing whose matrix element will become larger with increasing vibrational quantum number. Although the anharmonic Coriolis coupling coefficient in the present work is relatively small, the levels are essentially completely mixed for $J > 30$.

References

[1] K. Nakagawa, M. de Labachelerie, Y. Awaji, M. Kourogi, J. Opt. Soc. Am. B 13 (12) (1996) 2708–2714.
[2] C.S. Edwards, G.P. Barwood, H.S. Margolis, P. Gill, W.R.C. Rowley, J. Mol. Spectrosc. 234 (2005) 143–148.
[3] G. Herzberg, F. Patat, J.W.T. Spinks, Nature 133 (1934) 951.
[4] A. McKellar, C.A. Bradley Jr., Phys. Rev. 46 (1934) 664–666.
[5] C. Latrasse, M. Breton, M. Têtu, N. Cyr, R. Roberge, B. Villeneuve, Opt. Lett. 19 (22) (1994) 1885–1887.
[6] J. Lievin, M.A. Temsamani, P. Gaspard, M. Herman, Chem. Phys. 190 (1995) 419–445.
[7] L. Fusina, F. Tamassia, G. Di Lonardo, Mol. Phys. 103 (19) (2005) 2613–2620.
[8] M. Herman, C. Depiesse, G.Di. Lonardo, A. Fayt, L. Fusina, D. Hurtmans, S. Kassi, M. Mollabashi, J. Vander Auwera, J. Mol. Spectrosc. 228 (2004) 499–510.
[9] J.S. Muenter, V.W. Laurie, J. Am. Chem. Soc. 86 (18) (1964) 3901–3902.
[10] G. Wlodarczak, J. Demaison, J. Burie, M.C. Lasne, Mol. Phys. 66 (3) (1989) 669–673.
[11] M. Reich, R. Schieder, H.J. Clar, G. Winnewisser, Appl. Opt. 25 (1986) 130–135.
[12] R. El Hachtouki, J. Vander Auwera, J. Mol. Spectrosc. 216 (2002) 355–362.
[13] D.B. Moss, Z. Duan, M.P. Jacobson, J.P. O'Brien, R.W. Field, J. Mol. Spectrosc. 199 (2) (2000) 265–274.
[14] M. Herman, A. Campargue, M.I. El Idrissi, J. Vander Auwera, J. Phys. Chem. Ref. Data 32 (3) (2003) 921–1361.
[15] M.A. Temsamani, J. Vander Auwera, M. Herman, Mol. Phys. 79 (1993) 359–371.
[16] W.C. Swann, S.L. Gilbert, J. Opt. Soc. Am. B 17 (2000) 1263–1270.
[17] J.M. Brown, J.T. Hougen, K.P. Huber, J.W.C. Johns, I. Kopp, H. Lefebvre-Brion, A.J. Merer, D.A. Ramsay, J. Rostas, R.N. Zare, J. Mol. Spectrosc. 55 (1975) 500–503.
[18] T. Arusi-Parpar, R.P. Schmid, R.J. Li, I. Bar, S. Rosenwaks, Chem. Phys. Lett. 268 (1997) 163–168.